Published in final edited form as:
Birth Defects Res A Clin Mol Teratol. 2012 February ; 94(2): 102–113. doi:10.1002/bdra.22878.

Craniofacial Features Resembling Frontonasal Dysplasia with a Tubulonodular Interhemispheric Lipoma in the Adult 3H1 *tuft* Mouse

Keith S. K. Fong[1], **Tiffiny Baring Cooper**[1,3], **Wallace C. Drumhiller**[1], **Jack Somponpun**[1], **Shiming Yang**[1], **Thomas Ernst**[2], **Linda Chang**[2], and **Scott Lozanoff**[1]

[1]Department of Anatomy, Biochemistry & Physiology, University of Hawaii John A. Burns School of Medicine, Honolulu, HI

[2]Department of Radiology, University of Hawaii John A. Burns School of Medicine, Honolulu, HI

[3]Department of Radiation Oncology, University of Alabama at Birmingham, Birmingham, AL

Abstract

Intracranial lipomas are rare, but 45% of them occur along the midline cisterns between the hemispheres and are often associated with corpus callosum hypoplasia and craniofacial defects. They are difficult to detect, as they are generally asymptomatic and visible by MRI or by postmortem examination. The exact cause of these interhemispheric lipomas is not known, but they arise from a developmental defect resulting in the maldifferentiation of mesenchymal cells into mesodermal derivatives that are not normally present. We have identified a new mouse mutant called *tuft*, exhibiting a forebrain, intracranial lipoma with midline craniofacial defects resembling frontonasal dysplasia (FND) that arose spontaneously in our wild-type 3H1 colony. The *tuft* trait appears to be transmitted in recessive fashion, but approximately 80% less frequent than the expected Mendelian 25%, due to either incomplete penetrance or prenatal lethality. MRI and histological analysis revealed that the intracranial lipoma occurred between the hemispheres and often protruded through the sagittal suture. We also observed a lesion at the lamina terminalis that may indicate improper closure of the anterior neuropore. We have mapped the *tuft* trait to within an 18 cM region on mouse chromosome 10 by microsatellite linkage analysis and identified several candidate genes involved with craniofacial development and cellular differentiation of adipose tissue. *tuft* is the only known mouse model for midline craniofacial defects with an intracranial lipoma. Identifying the gene(s) and mutation(s) causing this early developmental defect will help us understand the pathogenesis of FND and related craniofacial disorders.

Keywords

intracranial lipoma; craniofacial defect; hypertelorism; corpus callosum; interfrontal bone

INTRODUCTION

Intracranial lipomas are abnormal masses of adipose tissue within the brain. They account for less than 1% of all brain lesions, but 45% of them occur along the midline axis between the cerebral hemispheres, typically within the pericallosal cistern, thus resulting in dysgenesis of the corpus callosum (Jabot et al., 2009). These interhemispheric lipomas can

Correspondence: Keith S. K. Fong, Ph.D., Department of Anatomy, Biochemistry & Physiology, University of Hawai'i John A. Burns School of Medicine, 651 Ilalo Street; BSB 110, Honolulu, HI 96813, ksfong@hawaii.edu, 808-692-1421.

be benign and asymptomatic, but many have been associated with patients suffering from persistent headaches, epileptic seizures, behavioral disorders, dysraphic lesions and midline craniofacial defects (List et al., 1946; Zee et al., 1981; Demaerel et al., 1996; Yildiz et al., 2006; Yilmaz et al., 2006). Surgical removal usually results in high morbidity and mortality due to strong adhesion to the surrounding tissue and the incorporation of cerebral arteries.

Interhemispheric lipomas are either curvilinear or tubulonodular. Curvilinear lipomas are thin and situated along the longitudinal body of the corpus callosum (pericallosal lipomas), whereas tubulonodular lesions are round, longer than they are wide, and tend to be situated at or near the genu (Truwit and Barkovich 1990). Because of this rostral location, it is thought that tubulonodular lipomas are formed at an earlier time point in development of the corpus callosum (Raybaud 2010). They vary in size, but can extend into the interhemispheric fissure and exit through the cranial sutures, presenting itself as an extracranial mass (Nordin et al., 1955; Zee et al., 1981; Kudoh et al., 1984; Nevin et al., 1999; Given et al., 2005). Tubulonodular lipomas are likely brought about by the delay or failure in resorption of the meninx primitiva along the dorsal midline of the developing telencephalon near the primitive lamina terminalis (Truwit and Barkovich 1990), but the exact cause is unknown. There have been a number of reports where craniofacial defects such as hypertelorism and median facial cleft, two characteristic features of frontonasal dysplasia (FND), have been observed together with tubulonodular lipomas (Pascual-Castroviejo et al., 1985; de Villiers et al., 1991; Tart et al., 1991; Demaerel et al., 1996, Wu et al., 2007).

FND or median cleft face syndrome comprises a variety of craniofacial defects that affect midline structures of the head. FND was first defined as having at least two of the following features, (1) ocular hypertelorism, (2) broadening of the nasal root, (3) median facial cleft affecting the nose, or both nose and upper lip or palate, (4) uni- or bilateral clefting of the ala nasi, (5) lack of formation of the nasal tip, (6) anterior cranium bifidum occultum, (7) V-shaped or widow's peak frontal hairline (DeMyer 1967, Sedano et al., 1970). Since then, various anomalies affecting the central nervous system, skeletal and cardiac systems have been observed along with features characteristic of FND, making it a heterogeneous group of developmental disorders. However, like all the other traits, the presence of a lipoma with FND was variable. It was observed in some subtypes of FND more than others, but never absolute in any one group (Wu et al., 2007). The significance of a lipoma in the formation or severity of FND is not clear. The occurrence of FND is rare and mostly sporadic. But, different modes of inheritance and genes have been identified in several FND subtypes (Wu et al., 2007, Uz et al., 2010). None of these models, however, includes a lipoma.

Mouse models have been useful systems for identifying genes and mechanisms crucial for proper craniofacial development (Copp 2006, Sandell et al., 2011). Recently, a new spontaneous mutant that we call *tuft* arose in our 3H1 wild-type mouse colony. Here we describe the craniofacial features that include a large midline lipoma erupting through the skull, ocular hypertelorism, and midfacial cleft, along with an interfrontal bone. Morphology of the basal forebrain region corresponding to the lamina terminalis was also abnormal, possibly indicating a defect during closure of the anterior neuropore. We have mapped the *tuft* trait to a region of mouse chromosome 10 that includes several loci associated with craniofacial anomalies and cellular differentiation. To our knowledge, *tuft* is the only mouse that models a midline intracranial lipoma together with craniofacial features characteristic of FND, thus providing a means to identify an element in the process of craniofacial development that is correlated with the pathogenesis of forming a lipoma.

METHODS

Animals and Breeding

All procedures were carried out in accordance with IACUC specifications and performed following protocols approved by the University of Hawaii Laboratory of Animal Services. Adult mice were housed under standard conditions with 12-hour light cycle and they were supplied with tap water and Rodent Mouse Chow *ad libitum*. The 3H1 strain was originally purchased from the MRC Radiobiolgical Laboratories (Didcot, UK) and has been inbred for over 40 generations since 1989 in our animal unit.

Magnetic Resonance Imaging

Seven adult mice (1 WT and 6 *tuft*) were scanned in a whole-body Siemens Trio 3 Tesla scanner, using a wrist receiver coil. Following a quick pilot acquisition, all animals were scanned in axial as well as sagittal orientation with a high-resolution 3D gradient echo sequence (TE/TR 7.4/14ms, 80mm FOV, in-plane resolution 250 × 250 microns, 0.5 mm slices, no gap, scan time 17:39 minutes). The T1-weighted sequence showed excellent contrast between the lipomas and surrounding brain tissue. A 2D T2-weighted spin-echo sequence was also acquired (TE/TR 70/5500ms, 83mm FOV, in-plane resolution 260×260 microns, 0.8 mm slices, 80 micron gap, scan time 16:55 minutes). Dicom images were subjected to 3D reconstruction utilizing Osirix (website). Resulting models were exported as .obj files, imported into Maya and partitioned and regionally enhanced by adding color and exported as .dxf format. The .dxf format was converted into .xdf and viewed utilizing SURFdriver software.

Whole Mount Staining

Whole mounts of crania were prepared following a modified technique of Inouye (1976). Crania were removed, brain tissue was extracted and heads were fixed in 95% ethanol. Cranial cartilage was stained with 0.3% Alcian blue (8GX). Specimens were dehydrated in 95% ethanol, counterstained with 0.1% Alizarin Red, macerated with KOH and cleared with increasing concentrations of glycerol. The sample consisted of 5 adult mice of both wild-type and affected animals. Each mouse cranium was observed with a Leitz dissection scope at 10X and 30X magnifications and cranial base cartilages and ossification centers were observed for their presence.

Histology and Immunohistochemistry

Five *tuft* mice displaying a lipoma were utilized for hematoxylin and eosin (H & E) histological analysis. Animals were sacrificed by an overdose of isofluorane, followed by decapitation. External tissue was removed from the head, keeping the skull intact and then fixed in 4% paraformaldehyde (PFA) overnight at 4°C. Samples were washed several times in phosphate buffered saline (PBS) and then decalcified with RDO solution according to the manufacturer's recommendations (Apex Engineering Products Corporation, Aurora, IL). Samples were subsequently washed in PBS and dehydration in increasing concentrations of ethanol to 70% and stored at 4°C. Samples were then embedded in paraffin and serially sectioned (10 μm) in a coronal or sagittal plane. Tissues were mounted on glass slides and stained with H & E using standard procedures.

Brain Fos expression—Identification of forebrain organuum vasculosum lamina terminalis (OVLT), supraoptic (SON) and paraventricular (PVN) neurons was determined by the expression of brain cFos as previously described (Somponpun and Sladek 2003). Briefly, ten mice (5 control and 5 *tuft*) were anesthetized with pentobarbital and perfused transcardially with physiological saline, followed by phosphate-buffered 4%

paraformaldehyde, pH 6.7 (Sigma, St. Louis, MO) after 48 hours of dehydration. After fixation, brains were removed and cryostat sections (40μM thick) were obtained in a one-in-four series and stored in cryoprotectant solution until processing. A single set of sections was used to localize Fos-immunoreactivity (-ir) in OVLT neurons. Cryoprotectant was removed from freely floating tissue sections with multiple rinses of 0.05 M buffered saline (KPBS, pH 7.4). The tissues were subsequently incubated with a rabbit polyclonal antiserum raised against amino acids 4–17 of human c-Fos (Ab-5, Calbiochem, San Diego, CA) at a 1:35,000 dilution prepared in KPBS with 0.4% Triton X-100 for 60 min at room temperature (RT), then 72h at 4°C. The sections were rinsed multiple times with KPBS, incubated with a biotinylated donkey anti-rabbit serum (Jackson ImmunoResearch, West Grove, PA) at a 1:600 dilution in KPBS with 0.4% Triton X-100 for 1h at RT. After several rinses, tissues were incubated in avidin-biotin complex solution for 1h at RT.

Primary antibody was localized using a conventional immunoperoxidase method with a 15-min exposure to nickel sulfate plus diaminobenzidine-HCl (Nickel II Sulfate + DAB) in sodium acetate solution in the presence of H_2O_2. This yielded a blue-black reaction product in the nuclear compartment. Sections were mounted on poly-L-lysine-treated slides, air-dried overnight, and coverslipped.

Cells that expressed nuclear blue-black immunoprecipitants after DAB-nickel reaction were considered positive. Fos expression was quantified in OVLT neurons following Ma and Lozanoff (1999). Briefly, a threshold was determined to remove background and the number of Fos-positive nuclei was determined in one or more sections from an arbitrarily selected specimen. The same threshold was applied to all sections of Fos-ir from all remaining specimens and stained cells were counted. For each variable, the mean value from multiple measurements from each animal was calculated, and these values were used to calculate group means that were compared utilizing a Student t test with a significance level of .01 (Sokal and Rohlf, 1981).

EMA and Vimentin staining—The staining for epithelial membrane antigen (EMA) and Vimentin (Santa Cruz Biotechnology, Santa Cruz, CA) were similarly processed using the avidin/biotin/peroxidase complex (ABC) technique as above. Sections were washed in KPBS at room temperature and incubated overnight at 4°C in a 1:1000 dilution of primary antibody. Sections were incubated in Nickel II Sulfate + DAB solution to reveal specific staining.

Genetic Analysis

Two sets of crosses were conducted to determine the location of the *tuft* locus by conventional linkage analysis using microsatellite markers. Once the mutant phenotype was indentified in the 3H1 wild-type colony, an inbreeding strategy was pursued to propagate the mutation. The 3H1 *tuft* mice were inbred for at least 8 generations by mating affected sibs, thus two inbred 3H1 lines, one called 3H1 wild-type and the other called 3H1 *tuft*. A concurrent outcross breeding strategy was performed to both BALB/c and Castaneus/Ei mice. Following the initial outcross, F1 mice were reciprocally backcrossed to affected 3H1 *tuft* mice. The numbers of affected and unaffected newborn or adult mice were recorded.

To localize the mutated locus, microsatellite linkage analysis was conducted. 3H1 *tuft* affected mice were out-crossed with BALB/c mice. The resultant 3H1 BALB *tuft* heterozygotes were then backcrossed to the 3H1 *tuft* affected parent to yield 3H1 BALB *tuft* affected animals for sampling (N2 mice). Specimens were scored at weaning, sacrificed, and DNA was extracted from tail tissue specimens. Microsatellite markers on chromosome 1, 2, 3, 4 and 10 were initially scored for backcross progeny (n=81). The markers included D1Mit90, D1Mit58, D2Mit63, D2Mit295, D2Mit200, D3Mit158, D3Mit203, D4Mit203,

D4Mit262, D4Mit12, D4Mit18, D10Mit238, D10Mit115, D10Mit230, and D10Mit134. Microsatellite primers were synthesized based on sequences listed at http://www.informatics.jax.org. Primer pairs were used to amplify each marker labeled with D4 (Beckman Coulter, Brea, CA) and Aplitaq Gold polymerase (Applied Biosystems, Carlsbad, CA) using a Perkin Elmer 9600 thermocycler with a PCR profile consisting of an initial 2 minute denaturing cycle at 94°C followed by 40 cycles for 30 seconds denaturing at 94°C, 30 seconds annealing at 50–58°C (depending on the primer set), and 30 seconds of extension at 72°C, followed by a final 4 minute cycle at 72°C. The D4-labelled PCR products were separated by CEQ 8000 capillary electrophoresis (Beckman Coulter, Brea, CA) according to the manufacturer's specifications. Recombinants were scored if *tuft* samples were heterozygous for 3H1 and BALB microsatellites. Data was analyzed using the Map Manager software (http://mcbio.med.buffalo.edu/mapmgr.html to estimate the location of the *tuft* locus relative to each marker. The Map Manager output was also used to identify likely data errors, such as close double recombinants. These were excluded from the analysis and the map process was repeated. A two-point LOD score analysis was conducted between all pairs of markers and the probable position of the *tuft* locus was calculated relative to surrounding microsatellite markers. A LOD score of greater than 3 was considered significant for linkage. Informative markers designed for subsequent linkage analysis restricted to Chr10 were TWD2 forward sequence: 5′-CGTTGCTGTGAGGACAATGC-3′, Reverse 5′-TGGTTCAGAGCCTGGTTTGG-3′ located 24.87 cM from the centromere and WD5 Forward sequence 5′-TCTGACATCTACATACATGC-3′, Reverse 5′-TAGGCTGAGAGATGCTAAGC-3′ located 45.54 cM from the centromere.

RESULTS

Phenotype of the adult tuft mouse

A mouse exhibiting ocular hypertelorism and a midline craniofacial lipoma spontaneously arose from our 3H1 wild-type colony, which we called *tuft*, because it had a mass of tissue that protruded through the top of the animal's head and was covered with fur (Fig. 1). The founder *tuft* mouse mated to 3H1 wild-type mice produced offspring that did not exhibit a phenotype, indicating that the *tuft* trait may be recessive. These inbred 3H1 F1 mice were backcrossed to the founder mouse, which generated a mixed progeny that did not follow the expected Mendelian ratio of inheritance. Only a few exhibited the *tuft* phenotype, while most did not (Table 1). The protruding mass was evident at birth and continued to grow in proportion to head size until the mouse matured. The mass varied in size, some very prominent while some very small or even not evident, except for a discolored patch of fur, demonstrating variable expressivity (Fig. 1E, F). Some mice had a midfacial cleft and hypertelorism (Fig. 1G, H). Each of these features appeared separately or together with one or more of the midline facial defects, which could be passed on to offspring exhibiting one or more of these traits, indicating incomplete penetrance.

The *tuft* phenotype was transmissible in outbred BALB/c and Castaneus/Ei mice. Upon outbreeding, affected offspring displayed hypertelorism while the lipoma was positioned at the midline with blanching of the overlying hair as observed in 3H1 *tuft* mice (data not shown). Inheritance of the *tuft* phenotype occurred at a rate of 23% based on inbred crosses (Table 1). No affected mice were produced in the F1 generation following reciprocal crosses between 3H1 *tuft* and either BALB/c or Castaneus/Ei mice, as would be expected for a recessive trait. Reciprocal backcrossing between 3H1 × BALB heterozygote animals with affected 3H1 *tuft* inbred mice produced 10% affected N2 offspring, which was less than expected for Mendelian inheritance of a recessive trait. The occurrence of *tuft* traits in 3H1 × Cast N2 adult mice was only 2/204 (0.98%) from 41 litters, thus attempts to backcross utilizing Castaneus was discontinued. Nonetheless, *tuft* was transferable to the Castaneus

background, although very rare. These data indicated that *tuft* shows incomplete penetrance and background strain effects on occurrence.

Magnetic Resonance Imaging and Histological Analysis Reveal an Intracranial Lipomatous Mass

Images generated using magnetic resonance (MRI) showed the occurrence of an intracranial lipoma in the midline cortical region, originating within the longitudinal fissure. The large mass protruding through the skull of an affected mouse (shown in Fig. 1C) appeared hyper-intense in both T1 and T2-weighted scans, which is consistent with adipose tissue (Fig. 2A–C). A darker, inner core was detected in the T1-weighted scan, but was nearly as bright and intense as the surrounding adipose in T2-weighted scans, suggesting the presence of cerebral spinal fluid (CSF). Three-dimensional modeling, based on reconstructed MR images, illustrated the midline position of the lipoma and its connection to the brain by meningeal extensions (Fig. 2D–G).

MRI of a mouse that did not have an extracranial mass (shown in Fig 1F) revealed a small, round lipoma situated at the midline between the cerebral hemispheres (Fig. 3A–C). Unlike the larger lipoma shown in Figure 2, it was not clear whether CSF infiltrated the smaller mass. Three-dimensional rendering of MRIs depicted the lipoma was nodular in shape and centrally positioned between the brain hemispheres (Fig. 3D–G).

Gross observation following dissection of affected animals such as the mouse shown in Figure 1C, revealed that the lipoma emerging from the brain and through a hole in the skull was attached to the dura (Fig. 4A). Histological analysis of coronal sections revealed a mass of differentiated adipose tissue emanating from the base of the longitudinal fissure, at the anterior region of the corpus callosum (Fig. 4B). The lipoma penetrated the brain parenchyma, but was sharply delineated by a ventral fibrous capsule consisting of mesodermal derivatives including dense connective tissue and occasional bone spicules and vessels. The capsule penetrating the parenchyma appeared to cut into the corpus callosum at the midline, but leaving the commissural fibers in either hemisphere intact.

Sections also showed that the dura underlying the cranium was intact and coursed outward and into the external mass through the skull, while the inner leptomeningeal layers were not distinguishable in the region of the capsule (Fig. 4C). However, other sections of affected mice clearly showed an inner meningeal layer coursing inward into the fissure and around the lipoma, suggesting that it may reside within the subdural space and originate from the leptomeninges at the level of the corpus callosum. It is unclear, however, whether the inner meningeal layers coursing into the brain includes the meningeal dura or just the leptomeninges. In either case, this association with the pia-arachnoid layers and central location at the level of the corpus callosum would expose the lipoma to the ventricular system. Gross aberrations of the lateral ventricles were also observed in some cases, revealing the disruptive affect by the lipoma (Fig 6B).

Higher magnifications of the dense tissue bordering the base of the lipoma appeared to be mainly composed of cells surrounded by dense fibrous material (Fig. 4C and D). We did not observe whorl formations within the fibrous capsule that are found in meningiomas (Louis et al., 2000). To determine whether the lipoma was of meningothelial origin, we assayed for the presence of vimentin and epithelial membrane antigen (EMA), two markers that are prominent in lipomatous meningiomas (Ohba et al., 2007). Immunohistochemical stains indicated that vimentin was present in the adipose, ependymal cells and fibrous-like tanycytes lining the third and lateral ventricles in 3H1 *tuft* mice, but neither in the fibrous capsule nor brain parenchyma as observed in lipomatous meningiomas (Fig. 5). Tanycytes and ependymal cells lining the lateral and third ventricles were also positive in sections from

the 3H1 background strain as expected for wild-type brains (Kameda et al., 2003). EMA was also negative in the fibrous capsule (data not shown), indicating that the lipoma did not derive from the meningothelia, but likely mesenchymal in origin.

Gross and Cellular Defect of the Lamina Terminalis

Brain morphology of the adult 3H1 *tuft* mouse revealed a lesion at the basal forebrain region corresponding to the lamina terminalis, exposing the third ventricle (Fig. 6A, B). To determine whether this lesion had an effect on the function of associated nuclei, we assessed the ability for adjacent osmoreceptors to sense changes in fluid balance by the expression of c-Fos protein in response to dehydration in five 3H1 *tuft* and five, 3H1 wild-type mice as controls. We saw a clear lesion in only one of the 3H1 *tuft* mice subjected to dehydration, but the number of c-Fos expressing cells in the organum vasculosum of the lamina terminalis (OVLT) was significantly less in each of them than similarly treated 3H1 wild-type mice ($p \leq 0.03$; Fig. 6C, D). Cell counts in the supraoptic nucleus (SON) and paraventricular nucleus (PVN) were also similarly reduced in each *tuft* mouse examined (Data for PVN not shown). The reduced expression indicated the inability for osmoreceptors to sense changes in plasma osmolality.

Interfrontal Bone

The external surface of the frontal craniofacial region was examined for an interfrontal bone that is dominantly expressed in particular strains of mice such as 3H1. The slender bone was positioned within the interfrontal suture and contacted nasal bones anteriorly and extended posteriorly to the transverse sinus (Fig. 7A). The incidence for an interfrontal bone in 3H1 wild-type mice was 100% (30/30) compared to a complete absence of expression in the same number of randomly sampled inbred BALB/c mice (Table 2). Each of the affected 3H1 *tuft* mice sampled, also had an interfrontal bone, but it was typically larger, diamond-shaped and much wider than those in the 3H1 wild-type strain (Fig. 7B). When 3H1 *tuft* was out-crossed with BALB/c wild-type mice, the occurrence of an interfrontal bone was 17% (5/30) in F1 offspring. Affected N2 animals (3H1 BALB *tuft*) backcrossed to 3H1 wild-type mice, however, typically had a larger interfrontal bone at an occurrence of 97% (29/30) when we expected a frequency closer to 50% if the expression for this trait was primarily due to the presence of the BALB/c background allele. These results indicated that the presence of an interfrontal bone was not only predominant in certain strains such as 3H1, but the factors that allow its expression were correlated with the *tuft* trait.

Linkage Analysis Identified a Region on Chromosome 10

Patterns of incomplete penetrance limited the linkage analysis to specimens collected from newborn or adult mice with visible defects. Thus, for the purpose of initially localizing a locus for the *tuft* mutation, all tested animals were assumed to have been homozygous for the 3H1 *tuft* allele and any recombination event occurring during meiosis would be indicated by the presence of amplimers for both the 3H1 and BALB strains (heterozygotes). Results for linkage to chromosome 1 using either the D1Mit90 or D1Mit58 markers turned out to be noninformative. Heterozygote frequencies for microsatellite markers on chromosomes 2, 3, and 4 were 53%, 56%, and 48% respectively, which indicated that the *tuft* mutation was not likely to be associated with these loci (data not shown). We also tested linkage to chromosome 10, since the *tuft* trait resembled the *Apaf1*^{fog} allele (Harris et al., 1997). A heterozygote frequency of 38.6% was obtained from 73 affected mice using the WD5 marker located near the *Apaf1* locus. We selected five other markers that were polymorphic for both 3H1 and BALB/c wild-type background strains along the chromosome to narrow the location of the *tuft* locus. Haplotypes for the 73 affected mice tested are shown (Fig. 8A). When analyzed using Map Manager, haplotypes were inferred for loci that couldn't be typed in some of the samples. The highest LOD score was obtained for the D10Mit115 marker,

which had a heterozygote frequency of 17.8% in 73 affected *tuft* mice (Bonferroni adjusted threshold $P = 0.0013$ for 40 chromosomes). Heterozygote frequencies of flanking markers (TWD2 and D10Mit230) increased as LOD scores decreased, suggesting a candidate region for the *tuft* locus circumventing the D10Mit115 marker, approximating 18 cM (Fig. 8B). The lower frequencies for heterozygotes at TWD2 and D10Mit115 than at distal markers D10Mit230, WD5, and D10Mit134 further indicated that the *tuft* locus is not likely near the *Apaf1* and *Alx1* loci.

DISCUSSION

Abnormal growth and differentiation of tissue are typical characteristics of tumors. Intracranial lipomas are not true neoplasms but heterotopic lesions caused by malformation of the leptomeninx during development (Kazner et al., 1980; Truwit and Barkovich 1990). These lipomas do not supersede the somatic growth of surrounding tissues. They actually incorporate intracranial vessels and even nerves, rather than displacing them. The extracranial portion of the lipoma in our *tuft* mice appears to grow in proportion to head growth, until the animals reach maturity. In some cases, the extracranial mass recedes over time. The reason for this is not known, but cessation of blood supply to the extracranial portion may have resulted from complete fusion of the cranial bones. Furthermore, the lipomatous mass consisted of mesodermal derivatives that were easily distinguishable and discriminated from the brain parenchyma. The fibrous capsule and adjacent parenchyma lacked whorl-like formations and positive staining for vimentin and EMA that are markers for lipomatous meningiomas (Louis et al., 2000; Ohba et al., 2007). This was not unexpected since meningiomas primarily manifest in adults. The lipoma in *tuft* was evident at birth, and was consistently localized within the meninges between the cerebral hemispheres by histology and MRI, indicating that it resulted from a defect occurring earlier during development.

Development of the cranial meninges begins as the neural tube is formed. A subset of mesenchymal cells from the neural crest migrate between the developing neuroepithelium and overlying ectoderm, beginning from about 9 days of gestation in the mouse, to form a primordial meningeal layer over the enclosing neural tube, called the meninx primitiva (McLone and Bondareff, 1975). The meninx differentiates into two layers, the outer pachymeninx gives rise to the dura and calvaria, while the inner leptomeninx develops into the pia-arachnoid layers. The pia-arachnoid layers are barely distinguishable, until about 13.5 days of gestation in the mouse, when the arachnoid separates into two layers by resorption of cellular material and dilation to form the subarachnoid space and cisterns, which is followed by the emergence of cerebrospinal fluid. Cavitation creating the subarachnoid space proceeds in an orderly fashion, beginning ventral of the brainstem and generally proceeds toward the anterior and dorsal regions of the brain (Osaka et al, 1980). A region dorsal to the primitive lamina terminalis is one of the last areas to be resorbed, and occurs just prior to closure of the sulcus medianus that form the massa commisuralis connecting the cerebral hemispheres. Thus, it has been postulated that the persistence of mesenchyme that failed to resorb, became vulnerable to maldifferentiation into ectopic mesodermal derivatives, such as adipose and dense connective tissue forming intracranial lipomas (Truwit and Barkovich 1990). The cause of persisting mesenchyme is unknown. However, coronal sections revealed that formation of the lamina terminalis (LT) was abnormal in some of our *tuft* mice. The cause for this is not known, but it may indicate a problem during closure of the rostral neuropore. On the other hand, this defect may be a secondary effect caused by the lipoma.

The LT is a thin membrane of grey matter that forms the anterior wall of the third ventricle and marks the closure site of the anterior neuropore (Puelles et al., 1987, Raybaud 2010). It

develops in association with neurons of the organum vasculosum of the lamina terminalis (OVLT), subfornical organ and median preoptic nucleus of the hypothalamus. Together, this forms the anteroventral third ventricle region (AV3V) that is able to sense and regulate fluid osmolality as it is exposed to the ionic and hormonal content of the systemic circulation due to an incomplete blood-brain-barrier (reviewed in McKinely et al., 2003). Lesions to the OVLT neurons render animals unable to detect changes in their plasma osmolality (Hochstenbach and Ciriello, 1996; Somponpun et al., 2004a, 2004b; McKinley et al., 2004). A result is the disruption of Fos expression from the vasopressin and oxytocin-producing neurons in the hypothalamus in response to plasma hypertonicity, as similarly observed in our *tuft* mice. This highlights the prominent role of the OVLT in electrolyte balance and suggests that *tuft* might not be able to do this effectively.

The defect seen at the LT may account for the craniofacial features of the *tuft* mouse. Improper closure of the neural tube in the cranial region can give rise to a host of skeletal and nervous system defects of varying degree (reviewed in Harding and Copp 2008). Neural crest cells migrating from the rostral part of the neural tube gives rise to the connective tissue and craniofacial skeleton of the head (reviewed in Le Douarin et al., 2007). Craniofacial defects are largely attributed to defects in neural crest cell formation, migration or differentiation (Trainor, 2005; Allam et al., 2011). Ocular hypertelorism and midfacial cleft exhibited by *tuft* are midline defects similarly observed in craniofrontonasal syndrome (CFNS) and FND. CFNS has been linked to mutations in the *EFNB1* gene (Twigg et al., 2004), while mutations in the *ALX1*, *ALX3* and *ALX4* genes result in variations of FND (Kayserili et al., 2009, Twigg et al., 2009, Uz et al., 2010). Similar defects have also been attributed to a reduction in *Six2* expression in *Brachyrrhine* (*Br/Br*) mice (Fogelgren et al., 2008). Each of these defects appeared to cause problems with neural crest cell proliferation and migration. A conditional knockout of the Kif3a intraflagellar transport protein resulted in aberrant neural crest cell proliferation at the facial midline, resulting in craniofacial defects characteristic of FND (Brugmann et al., 2010). The craniofacial defects seen in adult *tuft* mice appear to be relatively mild in comparison to CFNS and FND, but consistent with cases associated with the presence of a frontal lipoma or agenesis of the corpus callosum (DeMyer, 1967). In the case of FND, it is thought that a frontal lipoma could interfere with development of the nasal capsule, causing hypertelorism and bifid nose (Cohen, 2002). Although this is not clear to be the case in *tuft* mice, expression or lack of expression in these mice affected the size and shape of the interfrontal bone. The process of neural tube closure may influence these traits since modifications to the size and shape of the interfrontal bone has been correlated in mice with neural tube defects (Johnson, 1976).

The inferfrontal bone was first described as a slender osseous inclusion separating the anterior position of the frontal bones (Keeler, 1933). This structure is a quasi-continuous trait that shows variable occurrence in different strains of mice (Truslove, 1952). In this study, a sample of inbred 3H1 *tuft* mice displayed 100% occurrence of an interfrontal bone. The interfrontal bone in these skulls was larger and wider than the 3H1 wild-type background strain, with complex Wormian bones proximal to the exit hole for the extracranial lipoma. The lipoma probably presented a mechanical barrier restricting normal suture formation joining the cranial bones. It has been shown that defective meningeal development can impede calvarial bone osteogenesis (Opperman et al., 1995; Vivatbutsiri et al., 2008). Thus the abnormal sutural arrangement could be due, in part, to defective meningeal formation altering the expression of relevant osteogenic promoting genes such as *Sox9* for the posterior frontal suture (Sahar et al., 2005) or *Msx1* for the interfrontal suture (Satokata and Maas, 1994).

There are a number of loci on chromosome 10 with known mutations presenting craniofacial anomalies. Most notable is the *Alx1* gene, or cartilage homeoprotein 1 (*Cart1*). Mutations

were recently mapped to the *ALX1* gene in individuals with FND-like traits (Uz et al., 2010). Functional deletion of the *Alx1* gene resulted in apoptosis of head mesenchymal cells that caused improper neural tube closure in mouse embryos (Zhao et al., 1998). Also, the loss of functional Apaf1 apoptosis promoting protein resulted in mice with ectopic masses on their forehead, cauliflower like mass on the face, or exencephaly in E12.5 embryos due to improper closure of the neural tube (Harris et al. 1997, Yoshida et al., 1998). However, our linkage analysis seems to indicate that the *tuft* locus is further from either *Apaf1* or *Alx1* loci, since LOD scores for nearby markers were less than 1. Furthermore, mutations in neither of these genes resulted in a lipomatous mass as seen in the *tuft* mouse. There are a number of other loci within the 18 cM region between the TWD2 and D10Mit230 markers that may be attributed to the *tuft* traits, but it is too large a region to speculate candidate genes.

There are a number of disorders that manifest craniofacial defects together with forebrain anomalies. Intracranial lipomas have been associated with craniofacial disorders, but their etiology has not been elucidated or clearly delineated from cases with overlapping defects (Cohen, 2002; Castori et al., 2007). The *tuft* mouse is the only known animal that models an intracranial lipoma with craniofacial defects and closely resembling traits exhibited by the isolated form of FND (Wu et al., 2007). It is unclear how these abnormalities are correlated, but the defects may have resulted in a disruption of cellular signals between the forebrain and face during craniofacial morphogenesis. This may be determined by examining when these defects arise during embryogenesis. Expression analysis of candidate genes can lead to understanding which developmental pathways are disrupted during head development. Identifying the gene and its mutation that arose spontaneously in *tuft*, could lead to a gene affected in clinical cases with intracranial lipomas as well as elucidate the pathogenesis of FNDs.

Acknowledgments

This work was supported by The Hawai'i Community Foundation (08PR-43034 to K. Fong and 08PR-43033 to J. Somponpun), the National Institutes of Health (NCRR 5P20RR024206 to J. Somponpun and 1R01-DK-064752 to S. Lozanoff), the Infrastructure support from the National Center for Research Resources (G12RR003061 to G. Ostrander, Activity-Leader: T. Ernst), and the Specialized Neuroscience Research Program grant (U54NS056883 to L Chang). We would also like to extend our thanks to Renat Yakupov for assisting with the MR scanning.

References

Allam KA, Wan DC, Kawamoto HK, Bradley JP, Sedano HO, Saied S. The spectrum of median craniofacial dysplasia. Plast Reconstr Surg. 2011; 127(2):812–821. [PubMed: 21285785]

Brugmann SA, Allen NC, James AW, Mekonnen Z, Maden E, Helms JA. A primary cilia-dependent etiology for midline facial disorders. Hum Mol Genet. 2010; 19(8):1577–1592. [PubMed: 20106874]

Castori M, Rinaldi R, Bianchi A, Caponetti A, Assumma M, Grammatico P. Pai syndrome: first patient with agenesis of the corpus callosum and literature review. Birth Defects Res A Clin Mol Teratol. 2007; 79(10):673–679. [PubMed: 17803202]

Cohen MM. Malformations of the craniofacial region: evolutionary, embryonic, genetic, and clinical perspectives. Am J Med Genet. 2002; 115:245–268. [PubMed: 12503119]

Copp, AJ.; Greene, NDE.; Murdoch, JN. Mouse mutants as models of neural tube defects. In: Wyszynski, DF., editor. Neural Tube Defects From Origin to Treatment. New York: Oxford Univ Press; 2006. p. 198-213.

DeMyer W. The median cleft face syndrome: differential diagnosis of cranium bifidum occultum, hypertelorism, and median cleft nose, lip, and palate. Neurology. 1967; 17:961–971. [PubMed: 6069608]

de Villiers JC, Cluver PF, Peter JC. Lipoma of the corpus callosum associated with frontal and facial anomalies. Acta Neurochir Suppl (Wien). 1991; 53:1–6. [PubMed: 1803864]

Demaerel P, Van de Gaer P, Wilms G, Baert AL. Interhemispheric lipoma with variable callosal dysgenesis: relationship between embryology, morphology, and symptomatology. Eur Radiol. 1996; 6:904–909. [PubMed: 8972330]

Fogelgren B, Kuroyama MC, McBratney-Owen B, Spence AA, Malahn LE, Anawati MK, Cabatbat C, Alarcon VB, Marikawa Y, Lozanoff S. Misexpresion of Six2 is associated with heritable frontonasal dysplasia and renal hypoplasia in 3H1 Br mice. Dev Dyn. 2008; 237:1767–1779. [PubMed: 18570229]

Given CA, Fields TM, Pittman T. Interhemispheric lipoma connected to subcutaneous lipoma via lipomatous stalk. Pediatr Radiol. 2005; 35:1110–1112. [PubMed: 15918051]

Harding, BN.; Copp, AJ. Malformations. In: Love, S.; Louis, DN.; Ellison, DW., editors. Greenfield's Neuropathology. New York: Oxford University Press; 2008. p. 335-479.

Harris BS, Franz T, Ullrich S, Cook S, Bronson RT, Davisson MT. Forebrain overgrowth (fog) in the mouse affecting neural tube development. Tertatol. 1997; 55:231–240.

Hochstenbach SL, Ciriello J. Effect of lesions of forebrain circumventricular organs on c-fos expression in the central nervous system to plasma hypernatremia. Brain Res. 1996; 713:17–28. [PubMed: 8724971]

Inouye M. Differential staining of cartilage and bone in fetal mouse skeleton by alcian blue and alizarin red s. Cong Anom. 1976; 16:171–173.

Jabot G, Stoquart-Elsankari S, Saliou G, Toussaint P, Deramond H, Lehmann P. Intracranial lipomas: clinical appearances on neuroimaging and clinical significance. J Neurol. 2009; 256:851–855. [PubMed: 19280105]

Johnson DR. The interfrontal bone and mutant genes in the mouse. J Anat. 1976; 121:507–513. [PubMed: 1018005]

Kameda Y, Arai Y, Nishimaki T. Ultrastructural localization of vimentin immunoreactivity and gene expression in tanycytes and their alterations in hamsters kept under different photoperiods. Cell Tissue Res. 2003; 314:251–262. [PubMed: 13680355]

Kayserili H, Uz E, Niessen C, Vargel I, Alanay Y, Tuncbilek G, Yigit G, Uyguner O, Candan S, Hamza Okur, Kaygin S, Balci S, Mavili E, Alikasifoglu M, Haase I, Wollnik B, Akarsu NA. ALX4 dysfunction disrupts craniofacial and epidermal development. Hum Mol Genet. 2009; 18(22):4357–4366. [PubMed: 19692347]

Kazner E, Stochdorph O, Wende S, Grumme T. Intracranial lipoma: Diagnostic and therapeutic considerations. J Neurosurg. 1980; 52:234–245. [PubMed: 7351564]

Keeler CE. Interfrontal – a heritable cranial variation in the house mouse. J Mammalogy. 1933; 14:75–76.

Kudoh H, Sakamoto K, Kobayashi N. Lipomas of the corpus callosum and the forehead, associated with a frontal bone defect. Surg Neurol. 1984; 22:503–508. [PubMed: 6495161]

Le Dourain NM, Brito JM, Creuzet S. Role of the neural crest in face and brain development. Brain Res Rev. 2007; 55:237–247. [PubMed: 17765317]

List CF, Holt JF, Everett M. Lipoma of the corpus callosum. Am J Roent Rad Therapy. 1946; 55(2): 125–134.

Louis, DN.; Scheithauer, BW.; Budka, H.; von Deimling, A.; Kepes, JJ. Meningiomas. In: Kliehues, P.; Cavenne, WK., editors. World Health Organization Classification of Tumours: Pathology and Genetics of Tumours of the Nervous System. New York: Oxford University Press; 2000. p. 176-184.

Ma W, Lozanoff S. A full color system for quantitative assessment of histochemical and immunological staining patterns. Biotec Histochem. 1999; 74(1):1–9.

McKinley MJ, McAllen RM, Davern P, Giles ME, Penschow J, Sunn N, Uschakov A, Oldfield BJ. The sensory circumventricular organs of the mammalian brain. Adv Anat Embryol Cell Biol. 2003; 172:1–122.

McKinley MJ, Mathai ML, McAllen RM, McClear RC, Miselis RR, Pennington GL, Vivas L, Wade JD, Oldfield BJ. Vasopressin secretion: osmotic and hormonal regulation by the lamina terminalis. J Neuroendocrinol. 2004; 16:340–347. [PubMed: 15089972]

McLone DG, Bondareff W. Developmental morphology of the subarachnoid space and contiguous structures in the mouse. Amer J Anat. 1975; 142:273–293. [PubMed: 1119412]

Nevin NC, Leonard AG, Jones B. Frontonasal dysostosis in two successive generations. Am J Med Genet. 1999; 87:251–253. [PubMed: 10564879]

Nordin WA, Tesluk H, Jones RK. Lipoma of the corpus callosum. Arch Neurol Psychiatry. 1955; 74:300–307. [PubMed: 13248287]

Ohba S, Yoshida K, Akiyama T, Ikeda E, Kawase T. Lipomatous meningioma. J Clin Neurosci. 2007; 14:1003–1006. [PubMed: 17240148]

Opperman LA, Passarelli RW, Morgan EP, Reintjes M, Ogle RC. Cranial sutures require tissue interactions with dura mater to resist osseous obliteration in vitro. J Bone Miner Res. 1995; 10:1978–1987. [PubMed: 8619379]

Osaka K, Handa H, Matsumoto S, Yasuda M. Development of the cerebrospinal fluid pathway in the normal and abnormal human embryos. Child's Brain. 1980; 6:26–38. [PubMed: 7351160]

Pascual-Castroviejo I, Pascual-Pascual SI, Perez-Higueras A. Fronto-nasal dysplasia and lipoma of the corpus callosum. Eur J Pediatr. 1985; 144:66–71. [PubMed: 4018105]

Puelles L, Domenech-Ratto G, Martinez-De-La-Torre M. Location of the rostral end of the longitudinal brain axis:review of an old topic in the light of marking experiments on the closing rostral neuropore. J Morphology. 1987; 194:163–171.

Raybaud C. The corpus callosum, the other great forebrain commissures, and the septum pellucidum: anatomy, development, and malformation. Neuroradiology. 2010; 52:447–477. [PubMed: 20422408]

Sahar DE, Longaker MT, Quarto N. Sox9 neural crest determinant gene controls patterning and closure of the posterior frontal cranial suture. Dev Biol. 2005; 280:344–361. [PubMed: 15882577]

Sandell LL, Iulianella A, Melton KR, Lynn M, Walker M, Inman KE, Bhatt S, Leroux-Berger M, Crawford M, Jones NC, Dennis JF, Trainor PA. A phenotype-driven ENU mutagenesis screen identifies novel alleles with functional roles in early mouse craniofacial development. Genesis. 2011; 49(4):342–359. [PubMed: 21305688]

Satokata I, Maas R. Msx1 deficient mice exhibit cleft palate and abnormalities of craniofacial and tooth development. Nat Genet. 1994; 6:348–356. [PubMed: 7914451]

Sedano HO, Cohen MM, Jirasek J, Gorlin RJ. Frontonasal dysplasia. J Pediactrics. 1970; 76(6):906–913.

Sokal, RR.; Rohlf, FJ. Biometry. New York: WH Freeman and Co; 1981.

Somponpun SJ, Sladek CD. Osmotic regulation of estrogen receptor-beta in rat vasopressin and oxytocin neurons. J Neurosci. 2003; 23(10):4261–4269. [PubMed: 12764114]

Somponpun SJ, Johnson AK, Beltz T, Sladek CD. Osmotic regulation of estrogen receptor-beta expression in magnocellular vasopressin neurons requires lamina terminalis. Am J Physiol Regul Integr Comp Physiol. 2004a; 286(3):R465–473. [PubMed: 14604844]

Somponpun SJ, Johnson AK, Beltz T, Sladek CD. Estrogen receptor-alpha expression in osmosensitive elements of the lamina terminalis: regulation by hypertonicity. Am J Physiol Regul Integr Comp Physiol. 2004b; 287(3):R661–669. [PubMed: 15142833]

Tart RP, Quisling RG. Curvilinear and tubulonodular varieties of lipoma of the corpus callosum: an MR and CT study. J Comput Assist Tomogr. 1991; 15(5):805–810. [PubMed: 1885799]

Trainor P. Specification of neural crest cell formation and migration in mouse embryos. Sem Cell Dev Biol. 2005; 16:683–693.

Truslove GM. Genetical studies on the skeleton of the mouse. V. 'Interfrontal' and 'Parted Frontals'. J Genet. 1952; 51:115–122.

Truwit CL, Barkovich AJ. Pathogenesis of intracranial lipoma; An MRI study in 43 patients. Amer J Roentgenol. 1990; 155:855–864. [PubMed: 2119122]

Twigg SRF, Kan R, Babbs C, Cochukova EG, Robertson SP, Wall SA, Morriss-Kay GM, Wilkie AOM. Mutations of the ephrin-B1 (EFNB1), a marker of tissue boundary formation, cause craniofrontonasal syndrome. Proc Natl Acad Sci USA. 2004; 101:8652–8657. [PubMed: 15166289]

Twigg SRF, Versnel SL, Nurnberg G, Lees MM, Bhat M, Hammond P, Hennekam RCM, Hoogeboom AJM, Hurst JA, Johnson D, Robinson AA, Scambler PJ, Gerrelli D, Nurnberg P, Mathijssen MJ, Wilkie OM. Frontorhiny, a distinctive presentation of frontonasal dysplasia caused by recessive

mutations in the ALX3 homeobox gene. Am J Hum Genet. 2009; 84:698–705. [PubMed: 19409524]

Uz E, Alanay Y, Aktas D, Vargel I, Gucer S, Tuncbilek G, von Eggeling F, Yilmaz E, Deren O, Posorski N, Ozdag H, Liehr T, Balci S, Alikasifoglu M, Wollnik B, Akarsu NA. Disruption of ALX1 causes extreme microphthalmia and severe facial clefting: expanding the spectrum of autosomal-recessive ALX-related frontonasal dysplasia. Am J Hum Genet. 2010; 86:789–796. [PubMed: 20451171]

Vivatbutsiri P, Ichinose S, Hytonen M, Sainio K, Eto K, Iseki S. Impaired meningeal development in association with apical expansion of calvarial bone osteogenesis in the Foxc1 mutant. J Anat. 2008; 212:603–611. [PubMed: 18422524]

Wu E, Vargevik K, Slavotinek AM. Subtypes of frontonasal dysplasia are useful in determining clinical prognosis. Am J Med Genet Part A. 2007; 143A:3069–3078. [PubMed: 17955515]

Yildiz H, Kakyemez B, Koroglu M, Yesildag A, Baykal B. Intracranial lipomas: importance of localization. Neuroradiology. 2006; 48:1–7. [PubMed: 16237548]

Yilmaz N, Unal O, Kiymaz N, Yilmaz C, Etlik O. Intracranial lipomas-a clinical study. Clin Neurol Neurosurg. 2006; 108:363–368. [PubMed: 15893874]

Yoshida H, Kong Y-Y, Yoshida R, Elia AJ, Hakem A, Hakem R, Penninger JM, Mak TW. Apaf1 is required for mitochondrial pathways of apoptosis and brain development. Cell. 1998; 94:739–750. [PubMed: 9753321]

Zee C-S, McComb JG, Segall HD, Tsai FY, Stanley P. Lipomas of the corpus callosum associated with frontal dysraphism. J Comp Assisted Tomography. 1981; 5(2):201–205.

Zhao Q, Behringer RR, de Crombrugghe B. Prenatal folic acid treatment suppresses acrania and meroanencephaly in mice mutant for the Cart1 homeobox gene. Nat Genet. 1998; 13:275–283. [PubMed: 8673125]

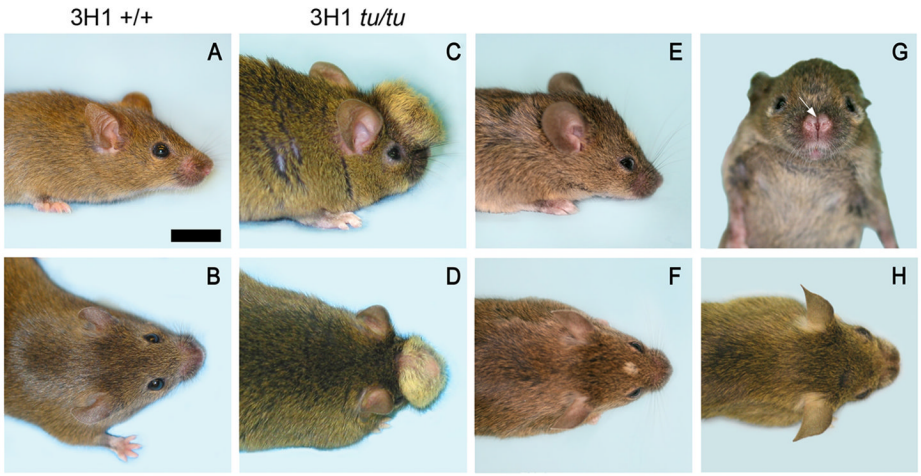

Figure 1.

Adult 3H1 wild-type mice viewed from **(A)** lateral and **(B)** superior perspectives. **(C–F)** Affected 3H1 *tuft* mice viewed from corresponding perspectives display a cranial lipoma as a mass variable in size protruding from the frontal area of the craniofacial region. **(G, H)** Affected 3H1 *tuft* mouse with midfacial cleft. Bar = 5.0 mm.

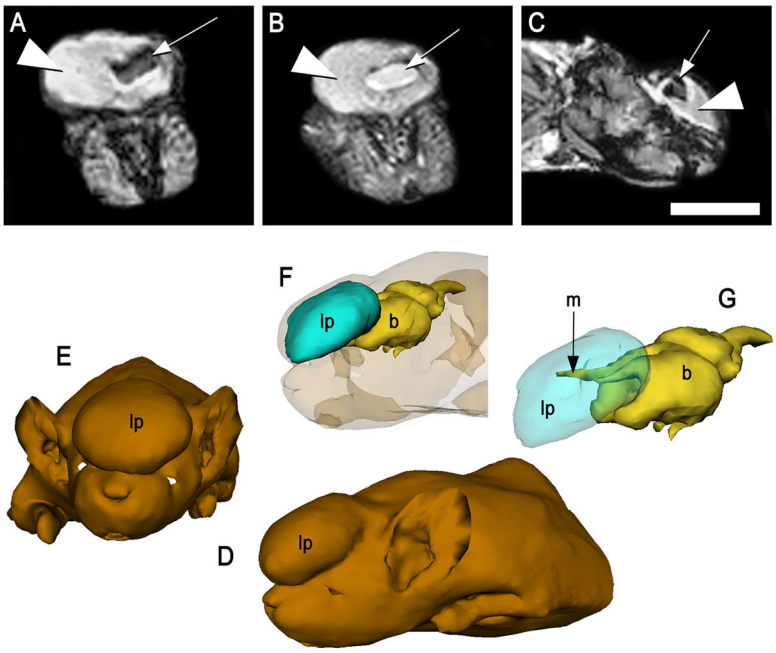

Figure 2.

MR scans of the affected 3H1 *tuft* mouse from Fig. 1C **(A)** Coronal T1-weighted and **(B)** T2-weighted, and **(C)** sagittal T1-weighted images, indicating the hyperintense protruding mass was consistent with adipose (large arrowhead), surrounding a central core of cerebrospinal fluid (small arrow). Bar = 5.0 mm. **(D–G)** 3D rendering of MRIs of the same specimen depicting the lipomatous mass (lp) was centrally positioned anterior and extended rostrally from the brain (b) via the meninges (m).

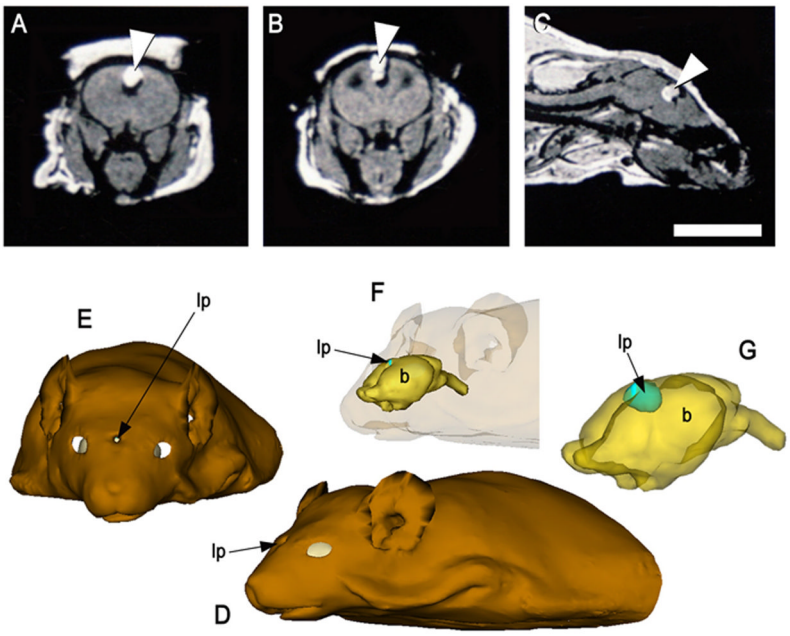

Figure 3.

MR scans of the affected 3H1 *tuft* mouse from Fig. 1E, showing a smaller cranial lipoma within the brain. **(A)** T1-weighted coronal view, **(B)** T2-weighted and **(C)** T1-weighted sagittal views, indicating a small mass consistent with adipose situated within the brain (arrowhead). Bar = 5.0 mm. **(D–G)** 3D rendering of MRIs depicting the lipomatous mass (lp) was nodular in shape and centrally positioned between the brain hemispheres.

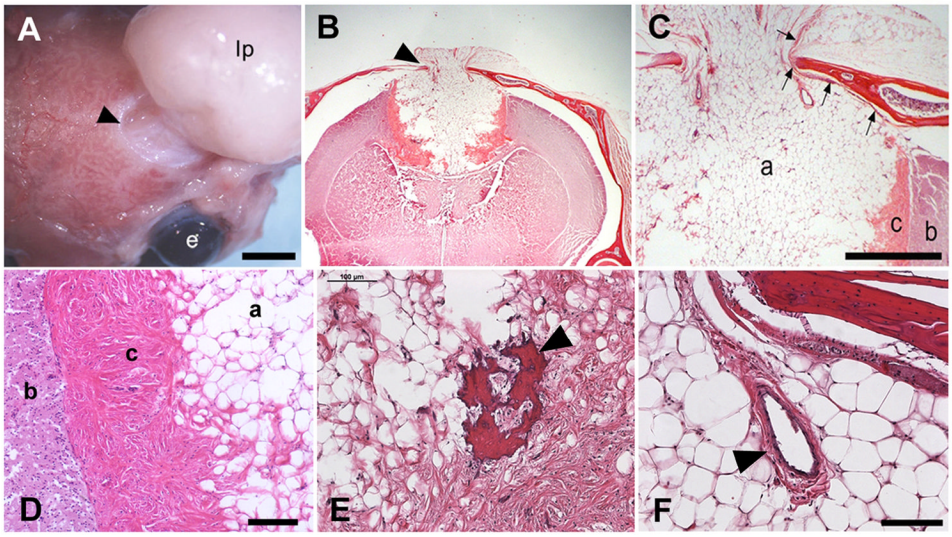

Figure 4.

Gross and histological analysis of affected 3H1 *tuft* mice. (A) Large, extracranial lipoma (lp) connected to the meninges through the exit foramen (arrowhead). Bar = 3 mm; e, eye. **(B)** Coronal histological section showing a large encapsulated cortical lipoma exiting the skull in the midline (arrowhead). **(C)** Higher magnification of (B) revealing the adipose (a) extending through the skull and was bordered by a distinct fibrous capsule (c) separating the mass from the brain parenchyma (b). Arrows point to the dura that lined and connected with the mass as it exited. Bar = 1.0 mm. **(D)** Higher magnification showing morphologies and boundaries separating the brain parenchyma (b), fibrous capsule (c) and adipose (a). Bar = 100 microns. **(E)** Bone spicule within the fibrous capsule (arrowhead). Bar = 100 microns **(F)** Blood vessel within the lipomatous mass (arrowhead). Bar = 100 microns

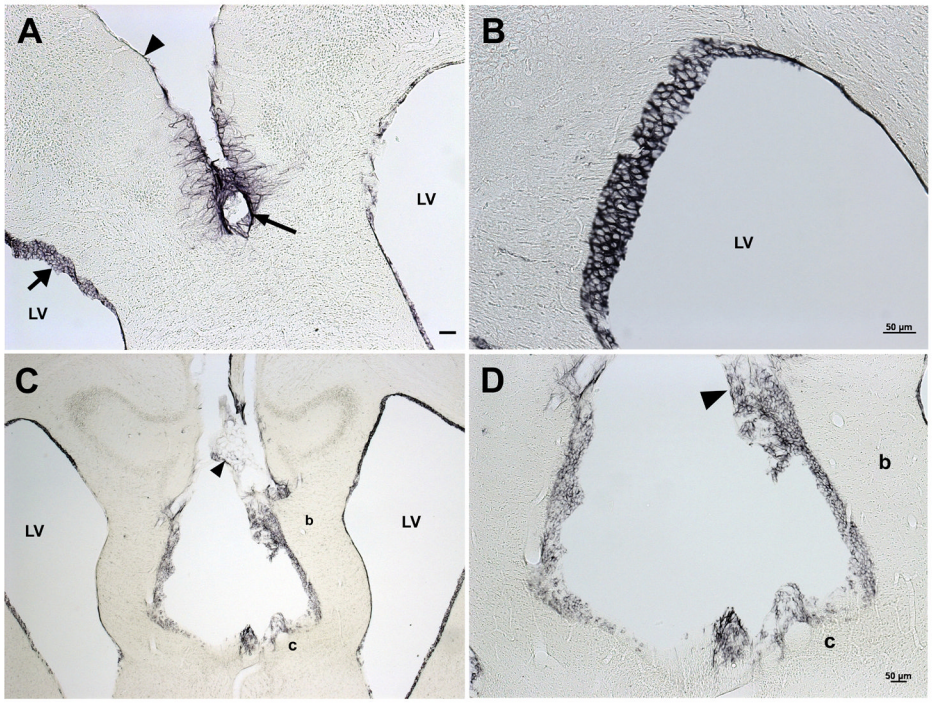

Figure 5.

3H1 wild-type and affected mouse brains immunostained for vimentin. **(A)** Coronal section of 3H1 wild-type positive for immunostaining staining vimentin in meninges (arrowhead), tanycytes (arrow) and ependymal cells (broad arrow) lining the lateral ventricles (LV). **(B)** Higher magnification of ependymal cells of the lateral ventricle from the 3H1 wild-type mouse shown in (A). **(C)** Affected 3H1 *tuft* immunopositive in adipose tissue of the interhemispheric lipoma (arrowhead), ependymal cells, but negative in the fibrous capsule (c) and brain parenchyma (b). **(D)** Higher magnification of lipoma in (C) showing positive staining for vimentin in adipose tissue (arrowhead) but negative in adjacent capsule (c) and parenchyma (b). Bar = 50 microns.

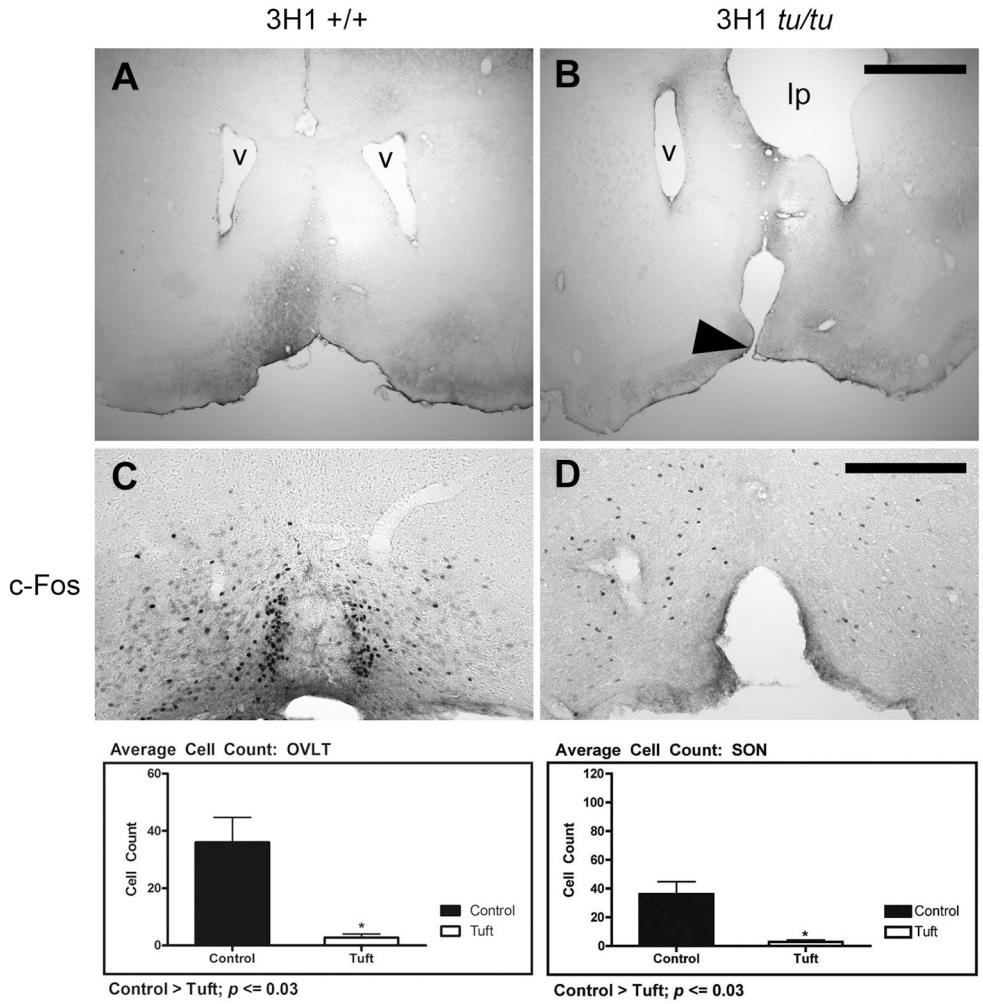

Figure 6.

Malformation of the lamina terminalis. **(A)** Coronal section of 3H1 wild-type at the level of the lateral ventricles with a normal lamina terminalis **(B)** 3H1 *tuft* showing discontinuity along the basal forebrain region corresponding to an abnormally formed lamina terminalis (arrowhead). Distorting effects on one of the lateral ventricles (v) by the intracranial lipoma (lp) was also revealed in one of the affected mice with a lipoma. Representative c-Fos immunostaining in **(C)** 3H1 wild-type and in **(D)** 3H1 *tuft* mouse serial sections from the mice in (A) and (B) respectively. **(Bottom)** Bar graphs illustrating the difference in cell numbers expressing c-Fos within the OVLT and SON averaged from a sample number of five. Bar = 1.0 mm for A and B. Bar = 200 microns for C and D.

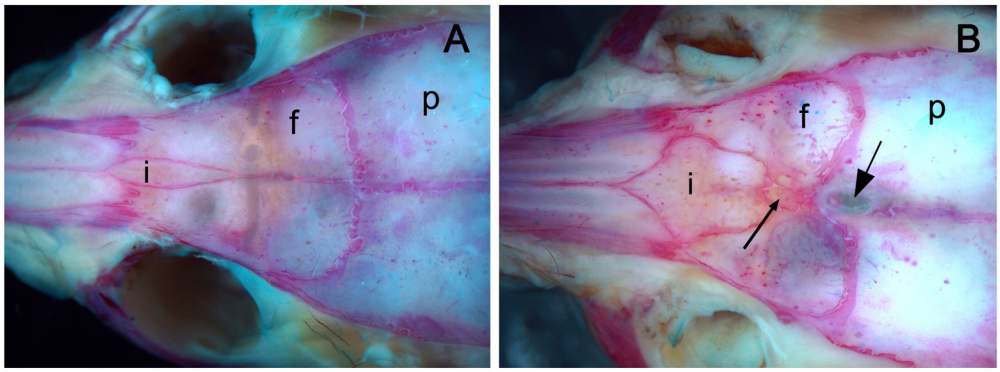

Figure 7.

Suture arrangement in **(A)** 3H1 wild-type and **(B)** 3H1 *tuft* mouse skulls stained with Alcian Blue and Alizarin Red. A distinct interfrontal bone (i) was present along the interfrontal suture between the two frontal bones (f) in the adult 3H1 wild-type (A), but broader and more prominent with complex Wormian bone formations (small arrow) in the 3H1 *tuft* (B). The exit foramen of the lipoma appeared between the parietal bones (p) just posterior of the bregma (intersection of the coronal and sagittal suture) in this example (large arrow).

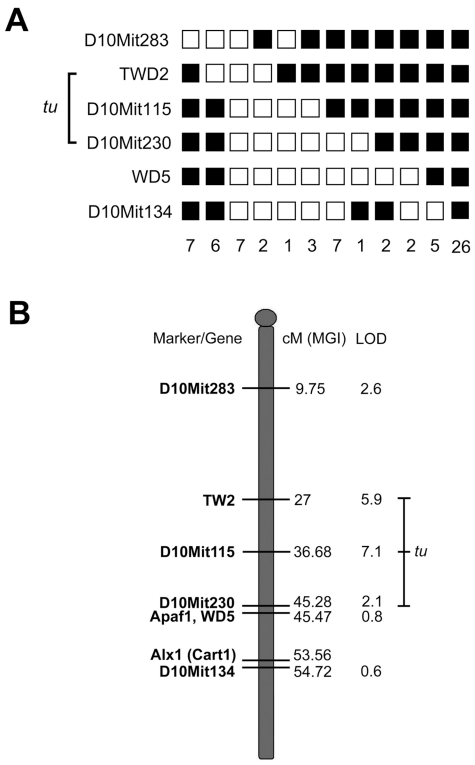

Figure 8.

Linkage map of a putative *tuft* locus on Chromosome 10. Genotype of microsatellite markers in 73 affected *tuft* N2 mice from a cross between 3H1 *tuft* and BALB/c **(A)** Each column represents a haplotype of Chr 10 markers. Filled boxes represent homozygosity for the 3H1 *tuft* allele and open boxes represent heterozygosity for the BALB/c allele. The number of mice with each haplotype is indicated at the bottom. Genotypes for four of the haplotypes were incomplete and remained uninformative, thus were not included. The range bar indicates a candidate region for the *tuft* locus. **(B)** Map of Chr 10 with putative *tuft* locus. From left to right, microsatellite markers and relevant genes, distance from the centromere in centiMorgans (cM) as reported by the Mouse Genome Informatics (MGI, 2011), and LOD scores. The range bar indicates the putative *tuft* locus between TWD2 and distal D10Mit230 markers.

Table 1

Inheritance of *tuft*/*tuft* postnatally based on outcross to BALB/c.

Cross	Total # of offspring	# affected	% affected	% expected if recessive	total # of litters
3H1 *tu/tu* × 3H1 *tu/tu* (INC)	140	32	23	100	39
3H1 *tu/tu* × BALB +/+ (OC)	55	0*	0*	0	15
3H1 *tu/tu* × 3H1×BALB *tu*/+ (BC)	359	36	10	50	70

*A 95% confidence interval of 0.0–5.82% is estimated for 0% occurrence in a sample size of 50 (Sokal and Rohlf, 1981).

IN = inbred cross; OC = outcross; BC = backcross.

Table 2

Inheritance of an interfrontal bone.

Strain and Cross	Iinterfrontal bone Presence/Total	%
3H1(IN stock)	30/30	100
BALB/c (IN stock)	0/30	0
3H1 × BALB F1 (OC)	5/30	17
3H1 × 3H1 BALB affected N2 (BC)	29/30	97
3H1 tu/tu (IN affected)	30/30	100

IN = inbred; OC = outbred cross; BC = backcross.